A New Tracer Advection Scheme for Bryan and Cox Type Ocean General Circulation Models

DUNCAN E. FARROW AND DAVID P. STEVENS

School of Mathematics, University of East Anglia, Norwich, United Kingdom

2 August 1994 and 28 November 1994

ABSTRACT

In regions with large tracer gradients and/or velocities the advection scheme that is used in many ocean models leads to significant under- and overshoot of the tracer values. In the case of the U.K. Fine Resolution Antarctic Model (FRAM), this lead to unphysical negative surface temperatures in some regions and overheating in others. In this paper, a new advection scheme is proposed and tested in the ocean model context using a limited-area model centered on a region where problems occurred in FRAM.

1. Introduction

The ocean is important in advecting heat from the Tropics to higher latitudes. Approximately a third of the total heat transported by the atmosphere and oceans toward the poles is carried by the oceans, and this heat is responsible for the temperature conditions on many of the surrounding continents such as Europe. It is thus essential that any changes in these transports are accurately modeled in climate forecast models. Furthermore, the feedback between the density field and ocean currents through the pressure means that advection of temperature and salinity is important for processes in ocean dynamics.

The tracer (e.g., temperature and salinity) advection scheme used by the U.K. Fine Resolution Antartic Model (FRAM) Group (1991) and other large-scale models (Bryan and Holland 1989; Semtner and Chervin 1992) has remained unchanged since the pioneering experiments of Bryan (1969). At the Geophysical Fluid Dynamics Laboratory (GFDL) Princeton, Bryan developed his model for coarse resolution experiments that the computers of the day dictated. The numerical scheme has survived the transition to high-resolution studies remarkably well. There have been a number of changes to the computer code to optimize its performance on vector-processing machines (cf. Semtner 1974; Cox 1984; Pacanowski et al. 1991). However, the finite-difference scheme, of what we will hereafter refer to as Bryan and Cox type models, has seen very little change. In the past when grid sizes were large, the eddy mixing coefficients (diffusion) were also large for numerical reasons. Thus, the effect of the advection scheme was limited, as the solutions were highly diffuse. As model resolutions have improved and the mixing coefficients have reduced in size, the advection scheme has become increasingly important. For instance, the advection scheme generally works well in the FRAM model (see Webb et al. 1991); however, in regions of strong gradients it can produce anomalous results. The worst examples occur in the region of the Agulhas Current and the Brazil/Falkland Current confluence. Figure 1 shows the surface temperature in the latter region as calculated by the FRAM project. There is significant under- and overshoot of the temperature with some neighboring grid points differing by tens of degrees and some single grid points having nonphysical negative temperatures. The situation is somewhat improved by the addition of nonphysical biharmonic mixing, which preferentially damps grid-scale waves. The degradation of the model results in this region are due to the advection scheme used in the tracer equations. The poor modeling of the advection of salt and temperature is doubly significant as there is a feedback via buoyancy into the momentum equations casting doubt on the accuracy of the velocity and pressure fields in the same region. The accurate modeling of advection in the momentum equations is not as important because the flow in the ocean is largely geostrophic and, hence, advection does not dominate the dynamics.

The advection scheme used in Bryan and Cox type models has a number of desirable properties that any advection scheme should possess. Uppermost is that it must conserve mass, and this is easily achieved if finite volume formulations are used. The scheme should also use explicit time integration since an implicit scheme is difficult to implement efficiently in a multiply connected domain such as the ocean.

Arakawa (1966) pointed out that any advection scheme should conserve the global second moment

Corresponding author address: Dr. Duncan E. Farrow, School of Mathematics, University of East Anglia, Norwich NR4 7TJ, England. E-mail: D.Farrow@uea.ac.uk

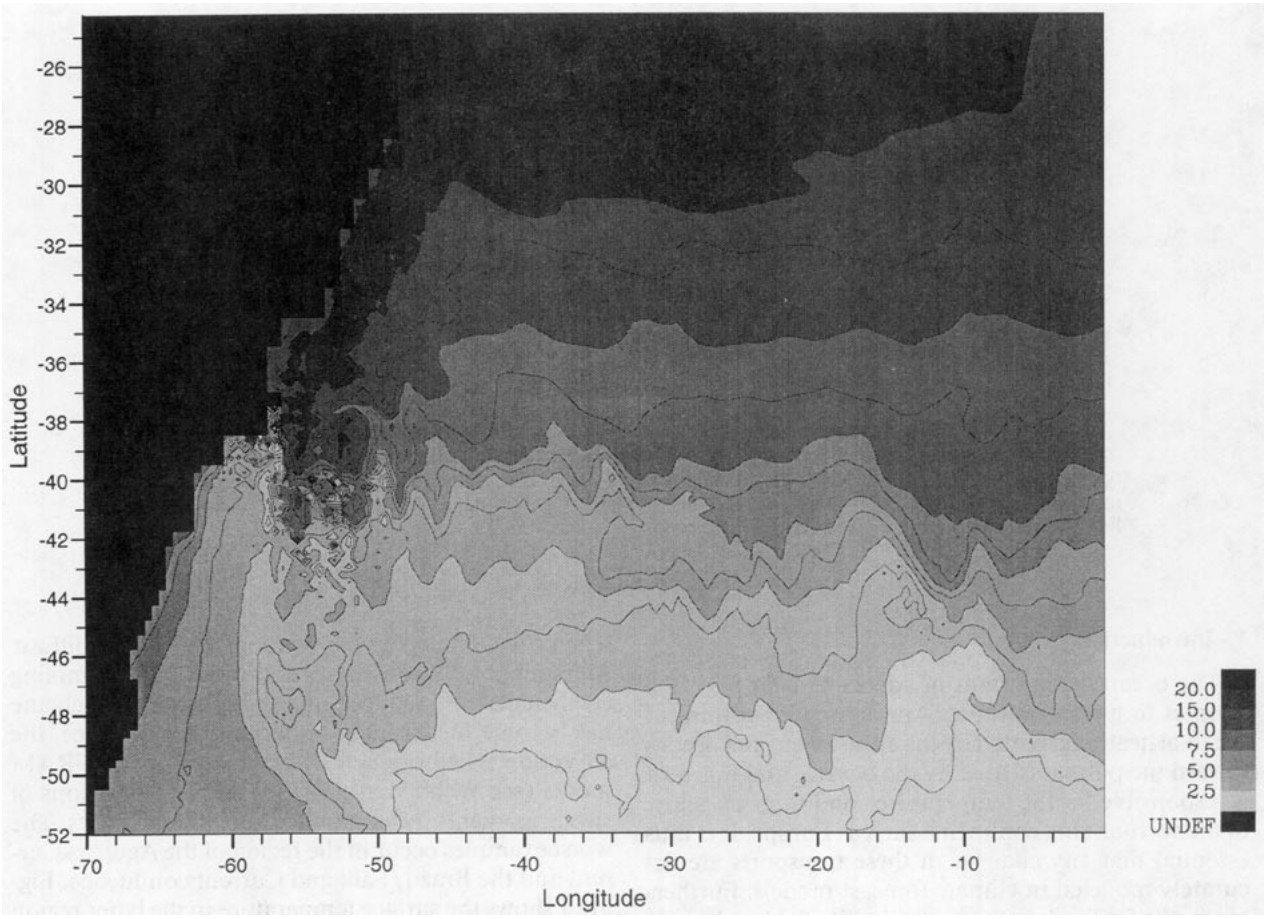

FIG. 1. An example of the output of FRAM for the surface temperature after 7 years of integration. There is significant under- and overshoot of the temperature near the South American coast.

(variance) of the advected quantity. This is especially important for the momentum equations where the variance is the kinetic energy. For tracer fields, a decrease in the total variance due to the advection scheme would represent numerical diffusion, which is undesirable and should certainly be much less than any physical diffusion. The advection scheme used in Bryan and Cox type models conserves the variance globally but not locally. However, this is at the expense of degradation of the solution due to numerical dispersion in regions where advection is dominating the physics like the area shown in Fig. 1.

Gerdes et al. (1991) investigated the influence of different advection schemes in an ocean model. In that paper three schemes were considered: upwind, the standard centered scheme, and the flux-corrected transport scheme of Boris and Book (1973). Gerdes et al. found that the choice of advection scheme had a significant effect on the northward heat transport in a North Atlantic model. They concluded that the upwind scheme, despite being positive definite, was too diffusive to be of practical use except in coarse-resolution models and that of the three schemes they considered, only the flux-corrected transport scheme succeeds in simulating a realistic equatorial thermocline.

The problem of accurately modeling advection is not limited to the area of oceanic modeling, and a number of recent review articles are available in the literature. Rood (1987) has reviewed a number of schemes in the closely related area of atmospheric modeling. Rood discussed many of the classical schemes as well as the flux-corrected transport schemes following the work of Boris and Book (1973). Patankar (1988) also reviews a number of advection schemes used in engineering (heat transfer and convection). Staniforth and Côté (1991) have reviewed the semi-Lagrangian approach in the atmospheric modeling context. A detailed discussion of advection in one dimension can be found in Leonard and Niknafs (1991).

In this paper, a new advection scheme is formulated that generates much less overshoot than the scheme used in previous Bryan and Cox type codes. The new scheme is described in section 2 where its properties are discussed in terms of advection in one dimension. In section 3, the new scheme is generalized to three dimensions and included in a limited-area ocean model

so that its performance can be evaluated in the ocean model context.

2. Advection schemes in one dimension

It is useful to discuss advection schemes in terms of numerically solving the one-dimensional advection equation for a tracer S,

$$\frac{\partial}{\partial t} S + u \frac{\partial}{\partial x} S = 0, \tag{1}$$

where u is a constant positive velocity. The exact solution to this equation is $S(x, t) = S(x - ut, 0)$; that is, the initial distribution of S is advected by u without any change in form.

Figure 2 shows a schematic of the advection scheme used in Bryan and Cox type models on a one-dimensional uniform grid. It is in a control volume form so that the flux out of one control volume must be a flux into a neighboring volume; thus, the method is guaranteed to conserve mass. The advective flux across one wall of the control volume is estimated using the average of the two values immediately to either side of the control volume wall. Using a leapfrog time integration scheme to obtain second-order accuracy in time yields the finite-difference equation

$$S_j^{n+1} = S_j^{n-1} - c(S_{j+1}^n - S_{j-1}^n), \tag{2}$$

where S is the quantity being advected, the superscript n refers to the time $n\Delta t$, the subscript j refers to the position in space $j\Delta x$, and $c = u\Delta t/\Delta x$ is the Courant number. This scheme is formally second-order accurate in space and time, and a Von-Neumann stability analysis shows that it is numerically stable for $c < 1$. The scheme also conserves the total variance of the advected quantity. This property of conserving the total variance can be carried over to nonuniform grids but at the cost of the scheme becoming first-order accurate in space. Note that the right-hand side of (2) does not depend on S_j^n, which leads to a checkerboarding of the solution; there are essentially two intertwined solutions evolving independently. In Bryan and Cox type models, this lack of dependence of neighboring grid points on each other is avoided by using an occasional mixing time step to smooth out grid-scale oscillations; however, this introduces some numerical diffusion and a consequent decrease in the total variance.

Figure 3 shows a schematic of a different advection scheme that is an adaptation of the QUICK scheme of Leonard (1979). Here, rather than use only those values that lie immediately to either side of a control volume wall, an extra value from upstream is used and the flux through that wall is a quadratic, rather than linear, interpolation. Unfortunately, simply substituting this quadratic form into the leapfrog or forward-time schemes yields methods that are computationally unstable. To maintain second-order accuracy a predictor–corrector time integration scheme is used with the predictor stage just using centered differences. This leads to the finite-difference equations for one time step integration

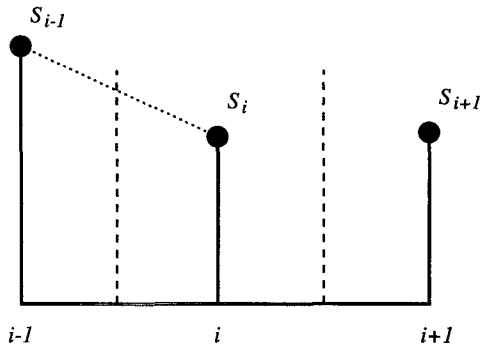

FIG. 2. Schematic of the standard advection scheme used in FRAM and other models.

$$S_j^{n+1/2} = S_j^n - \frac{c}{4}(S_{j+1}^n - S_{j-1}^n),$$

$$S_j^{n+1} = S_j^n - \frac{c}{2}\left(S_{j+1} - S_{j-1} - \frac{1}{4}(S_{j+1} - 3S_j + 3S_{j-1} - S_{j-2})\right)^{n+1/2}. \tag{3}$$

This scheme is third-order accurate in space and second order in time. A Von-Neumann stability analysis shows that the Fourier component amplitude factor in terms of the phase variable $\theta = k\Delta x$ is given by

$$G^2(\theta) = 1 + \frac{c}{4}(-\cos 2\theta + 4\cos\theta - 3) + \frac{c^2}{32}(\cos 3\theta + 2\cos 2\theta - 17\cos\theta + 14) + \frac{c^4}{512}(-3\cos 5\theta + 18\cos 4\theta + 25\cos 3\theta - 104\cos 2\theta - 22\cos\theta + 86). \tag{4}$$

From (4), it can be shown that $G^2 < 1$, for all θ if

$$c < \left(\frac{1}{4} + \frac{1}{36}\sqrt{29}\sqrt{3}\right)^{1/3} - \frac{1}{6}\left(\frac{1}{4} + \frac{1}{36}\sqrt{29}\sqrt{3}\right)^{-1/3}; \approx 0.5898 \tag{5}$$

thus, the new advection scheme has a tighter stability constraint than the usual CFL condition. The above scheme does not conserve the second moment and, in fact, introduces some numerical diffusion equivalent (in one dimension) to that introduced by the QUICKEST scheme (Leonard 1979). The importance of this will be discussed later when the new scheme is included in an ocean model.

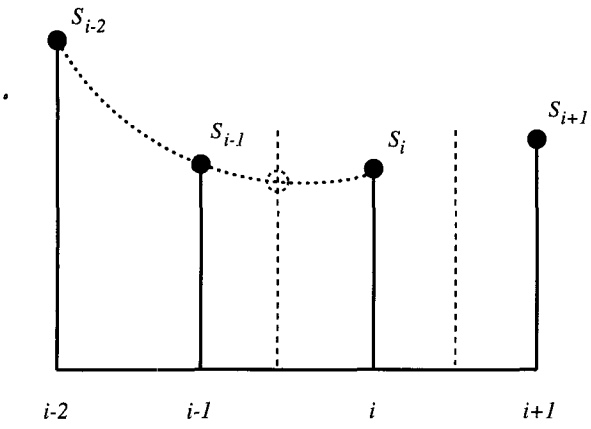

FIG. 3. Schematic of a new scheme based on the QUICK scheme of Leonard (1979).

Figure 4 shows how the two different schemes outlined above advect two different profiles in one dimension. Also included for comparison is a calculation using the highly diffusive upwind scheme (cf. Rood 1987). The problem is defined to be periodic. The Courant number is $c = 0.1$, and the figure shown is after 500 time steps with 80 points in space. For both profiles in Fig. 4, the standard scheme has seriously degraded the solution with dispersion leading to under- and overshoot. The position of the peak of the triangular profile is poorly predicted by the standard scheme as it significantly lags its true position. All the adverse effects on the solution can be attributed to the dispersion of the higher wavenumber modes. The total variance of the solution has been conserved to computational accuracy. The solution calculated by the new scheme behaves much better in terms of the under- and overshoot. The position of the peak of the triangular profile is more accurately estimated. There is a region of some under- and overshoot behind the rectangular profile reflecting the presence of some dispersion though it is less than that associated with the standard scheme. The total variance has dropped by about 7.5% indicating that there is some numerical diffusion. This is much less than the highly diffusive upwind scheme where the total variance has dropped by 53%. The importance of this numerical diffusion is dependent on how much explicit diffusion is included in any particular model. The significance of numerical diffusion in the ocean modeling context is discussed in detail later in this paper.

The new scheme has clear advantages in terms of the quality of the solution, at least in one dimension, over the leapfrog scheme. However, a one-dimensional test of an advection scheme is not sufficient to assess its suitability in an ocean modeling context; therefore, in the next section, a limited-area ocean model is examined using both the standard and new schemes.

The new scheme can readily be generalized to multiple dimensions by treating each component of the advective flux separately. The details are described in the appendix. The quadratic interpolation used to calculate the wall values carries over to nonuniform grids in a straightforward way. Close to a physical boundary, it is possible for the quadratic interpolation to require the value of a tracer outside of the computational domain. In this case, a linear interpolation is used.

3. "Real" ocean example

a. Model formulation

In this section, the numerical advection scheme discussed in the previous section is generalized to three dimensions and included in an array processor version of the Modular Ocean Model (Pacanowski et al. 1991) known as MOMA (Webb 1993). This code is then used to compute the flow in a limited region centered on an area where problems have been encountered in the FRAM project—namely, the Brazil and Falklands Currents confluence. The primary aim of the simulation is to evaluate the effectiveness of the new scheme in an oceanographic context with irregular topography and variable tracer fields and yet have a model that needs only modest computing facilities. The aim is not to accurately model the flow in this region. To this end, vertical walls are placed to the north, south, and east of the region at 52°S, 25°S and 0°W. Using the same resolution as the FRAM experiment—namely, a latitudinal grid scale of 0.25°—a longitudinal grid scale of 0.5° and vertical levels varying from 20 to 230 m, yields a 140 × 112 × 32-level computational domain. Placing solid walls where there were open ocean boundaries drastically alters the flow in this region; therefore, the flow was also calculated using the unaltered MOMA code—that is, with the standard advection scheme. The artificial vertical walls generate strong upwelling; therefore, for the purposes of maintaining numerical stability, it was found necessary to hold the

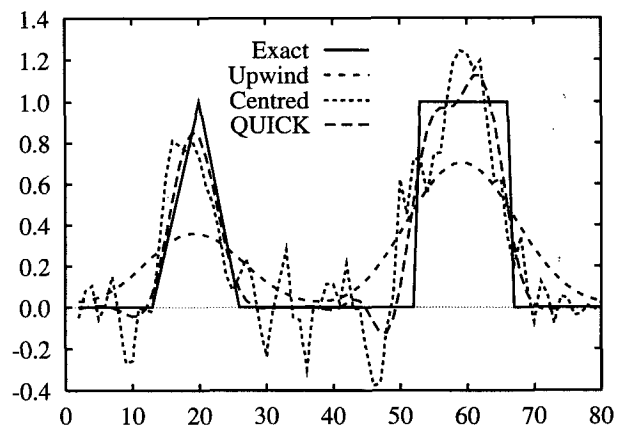

FIG. 4. An example of how various schemes advect two different profiles in one dimension. Here, $c = 0.1$, and there are 80 spatial grid points.

values of scalar quantities constant for 5 grid points in from the artificial walls. No such restriction was imposed on the temperature and salinity values next to the coast of South America. The two simulations were run for 300 days from rest with no surface fluxes or stresses. The initial temperature and salinity fields were set to the annual mean Levitus (1982) climatology. The only difference between the two codes is in the way that the tracer equations are integrated. The methods for calculating the barotropic streamfunction and velocity are unaltered as is the feedback between the tracer and momentum equations.

b. Results

Both salinity and temperature are included in the ocean model under consideration, but in this section, discussion will focus on temperature though all the conclusions are equally valid for salinity or indeed any other tracer. Figure 5 shows the surface temperature after 100 days from the two different simulations. The overall structure of the results does not differ greatly between the two codes. There is a strong western boundary current (WBC) that carries warmer waters from the northern part of the domain to the south. The presence of the artificial vertical wall at the southern boundary greatly influences the flow, so these results differ from those obtained from FRAM (see Fig. 1). It is the magnitude of the Falkland Current that is responsible for the location of the separation of the Brazil Current from the coast of South America (Matano 1993). However, because of the closed southern boundary, the Falkland Current is very much reduced in this model. What is not different, however, is the significant amount of under- and overshoot in the results of the unmodified code. The nature and magnitude of this degradation of the solution is similar to that observed in the results of FRAM for the same region (Fig. 1) though not quite as bad because of the reduced gradients in the confluence. The results of the modified code show no such degradation; the temperature field is generally much smoother. This does not appear to be at the expense of a significant amount of numerical diffusion since the width of the WBC is very much the same for both cases. Furthermore, instabilities associated with eddy formation are not damped and occur throughout the domain of both models. The importance of numerical diffusion in the current simulations will be discussed in more detail later. There are some small-scale structures, particularly at the edge of the WBC, that are not as pronounced in the results of the modified code but the form of these structures could be significantly influenced by the under- and overshoot generated by the standard advection scheme. Away from the strongly advecting WBC, the two sets of results are in good agreement although some of the grid-scale structures are absent in the modified model.

Figure 6 shows the difference between the two results quite dramatically. Here, a cross section of the surface temperature after 100 days from west to east across the computational domain at 39°S is shown. The warmer temperatures in the west are due to the northern waters being advected south by the WBC. The modified code produces a much smoother distribution of temperature than the unmodified code. The overshoot in the results of the unmodified code is as much as 5°C, which, in the WBC, leads to neighboring grid points differing by 10°C. This overshoot is of the same order as the underlying temperature structure due to the WBC and thus represents a significant degradation of the solution. At the same grid points, the modified code predicts a difference of less than 1°C. Again, away from the vigorously advecting WBC, the two codes produce results that are in good agreement.

Figures 5 and 6 illustrate how the results of the two different codes vary spatially. Figure 7 is a time series of the maximum surface temperature as calculated using the two codes. There are no surface fluxes in this model, and the initial temperature maximum occurs at the surface. Hence, there is no physical mechanism whereby the maximum surface temperature can increase with time; it should be less than or equal to the initial maximum of 24.14°C. The unmodified code produces maximum surface temperatures significantly greater than the initial value. This is entirely due to the overshoot associated with the advection scheme and is as much as 12°C (after 80 days) above the correct value. Note that the actual overshoot that produces this spurious maximum may be greater than 12°C if the maximum occurs at a point where the temperature should be less than 24.14°C. After some time, the overshoot has decreased in magnitude, so the maximum temperature is overestimated by approximately 3°C. This is due to the decreasing importance of advection in the dynamics as the model spins down. The maximum surface temperature of the modified code remains at 24.14°C except for a brief period near 150 days where there is an overestimation of about 0.5°C, demonstrating that the new advection scheme is not immune to overshoot. Overall, however, the new scheme has performed much better in this regard. A similar set of observations carry over to the minimum surface temperature, except that now upwelling and vertical diffusion are mechanisms whereby the minimum surface temperature can change with time. In Fig. 7, the minimum surface temperature is the same for both codes up to about 120 days after which the unmodified code has the minimum below the initial value. This drop occurs at about the same time as the warmer waters advected south by the WBC move into the region where the initial surface minimum occurred. The minimum surface temperature calculated by the modified code remains at its initial value. It is not clear whether lower minimum surface temperatures of the unmodified code are due entirely to undershoot. There may be some effect due to strong upwelling due to

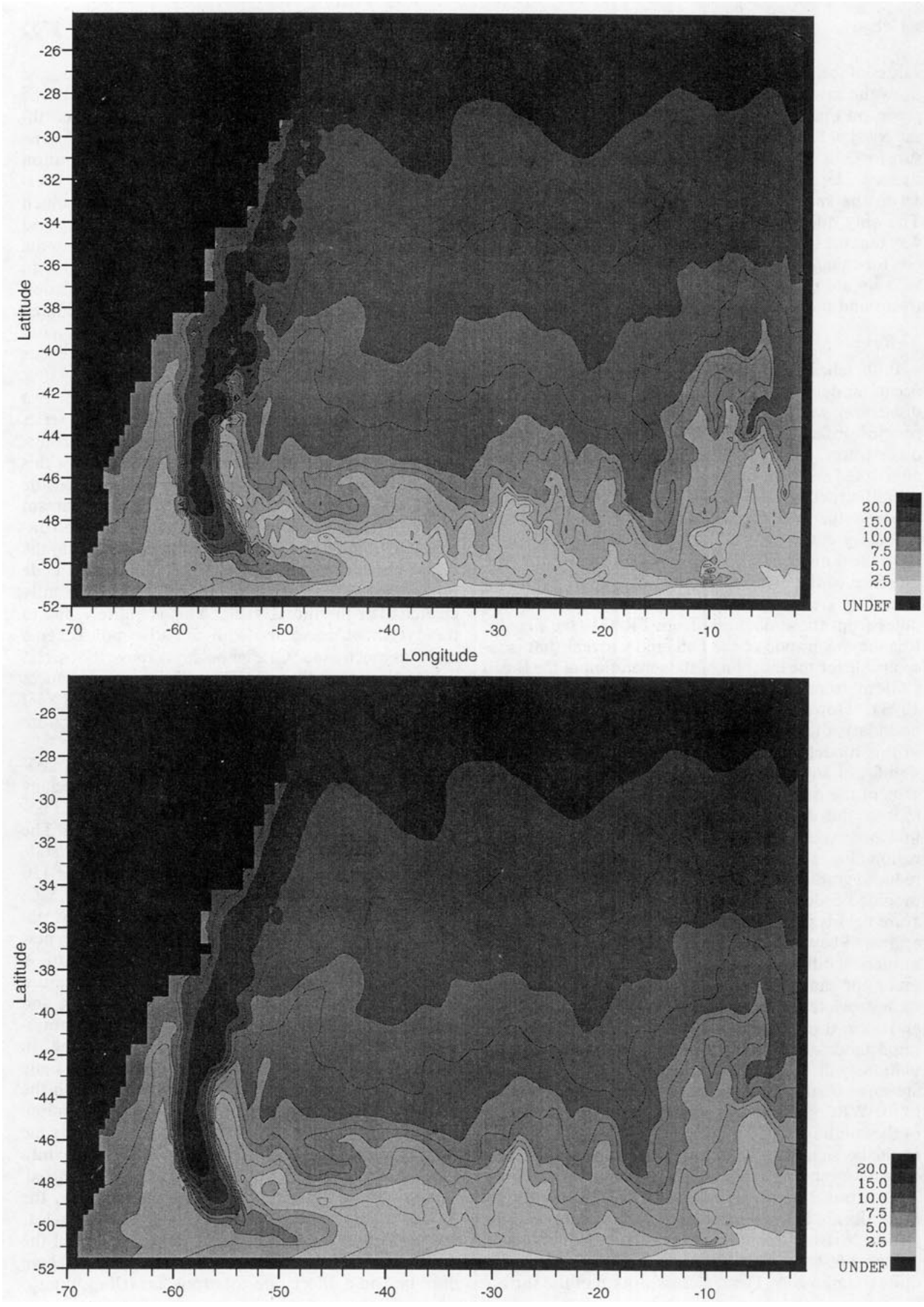
-26
-28
-30
-32
-34
-36
-38
-40
-42
-44
-46
-48
-50
-52
Latitude
-70
-60
-50
-40
-30
-20
-10
Longitude
20.0
15.0
10.0
7.5
5.0
2.5
UNDEF

Longitude

enhanced local horizontal buoyancy gradients associated with the standard advection scheme.

Figure 8 shows current vectors after 100 days as calculated by the unmodified and modified models. To improve the clarity, only that part of the computational domain that includes the WBC is shown. The striking difference between these two figures is that the results of the modified code show a much more coherent structure for the WBC. Since the same method is used to calculate the velocities in both codes, the difference can be due only to the degraded temperature and salinity fields that drive the momentum equations via pressure gradient. At some points in Fig. 8a, the velocities of neighboring grid boxes might be at right angles despite being of the order of 20 cm s^{-1}. Even if this were physical, the scale of this feature is too small to be properly resolved by the model.

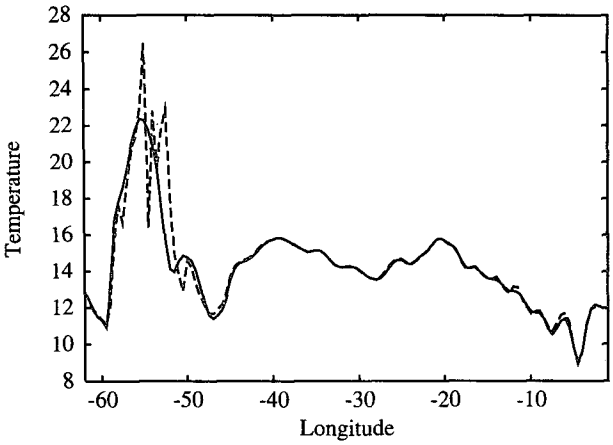

FIG. 6. Cross section at −39°N of the surface temperature at 100 days showing the difference between the results of the two codes. The solid line is for the modified model and the dashed is for the standard model.

c. *The role of numerical diffusion*

The improvement in appearance of the solutions discussed above is of little value if it has been at the expense of significantly enhanced numerical diffusion. Figure 9 shows a time series of the total variance of the temperature within the computational domain calculated by the two different codes. Because of the fixed values along the northern, southern, and eastern boundaries, there is a tendency for the second moment of temperature to increase with time. The boundaries at the vertical walls are acting like fixed temperature boundaries. Despite this, if there is a significant amount of numerical diffusion introduced by the new advection scheme, then the total variance calculated by the modified code should be consistently less than that calculated by the unmodified code. In fact, the opposite is the case, the results of the modified code are *greater* than those calculated by the unmodified code, indicating that there is more diffusion present in the unmodified code. This can be explained by the enhanced explicit diffusion that occurs in the unmodified code. It has already been noted that the overshoot generated by the standard advection scheme can lead to neighboring grid points differing by up to 10°C, whereas the modified code calculates the difference to be less than 1°C. These artificially large gradients lead to greatly enhanced explicit diffusion. This means that there is more diffusion in the results of the unmodified code than in those of the modified code, where such large overshoots do not occur. Thus, paradoxically, despite the fact that the new advection scheme introduces some numerical diffusion, the modified code appears to perform better in terms of the global variance of temperature than the unmodified code. It is interesting to note that most of the flow is in geostrophic balance, and thus the surface velocities are parallel to density contours. This has implications for numerical diffusion, which is greatest in the direction that fluid is being advected. If the flow is in near-geostrophic balance, this will be in a direction of low tracer gradient; hence, the significance of numerical diffusion will be less.

The conclusion that the modified model performs better in terms of the conservation of the second moment has been tested in a more idealized model. This model allowed a greater control of fluxes and could be run with and without explicit diffusion. The ocean model discussed above quickly becomes unstable if it is run without any explicit diffusion. The idealized model consists of a 26° × 10° rectangular domain. The region is uniformly discretized by a 52 × 26 grid with 15 levels in the vertical. Flow in the domain is driven by an initial temperature front across a north–south line dividing the domain into two equal halves. The initial temperature difference across the front was 10°C at the surface decreasing to 0°C at level 9.

Figure 10 shows time series for four different calculations of this idealized model with and without explicit diffusion using both the modified and unmodified codes. As expected, the results of the unmodified code without explicit diffusion conserve the total variance to computational accuracy. When there is some explicit diffusion present, the total variance decreases with time, reflecting that diffusion. For the modified code without explicit diffusion, there is an initial decay in the total variance due to numerical diffusion. This decay is quite rapid but is limited to the first day or so of the simulation after which there is a period of growth in the total variance indicating that the model is unstable.

FIG. 5. The surface temperature after 100 days as calculated by (a) the standard code and (b) the modified code.

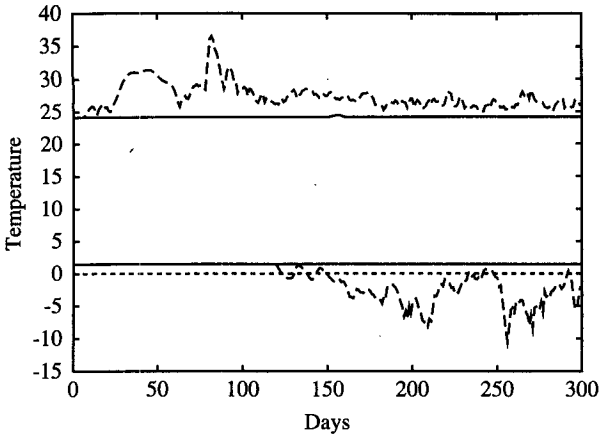

FIG. 7. Time series of the maximum and minimum surface temperature as calculated by the two models. The solid line is for the modified model and the dashed is for the standard model.

This instability disappears after about 25 days, and there is a gradual decay of the total variance due to numerical diffusion. The initial rapid decay is due to the large velocities that are produced across temperature gradients. Initially, neighboring grid points differ by up to 10°C. Over the timescale of a day, a geostrophic balance is set up that reduces the significance of numerical diffusion since velocity vectors are nearly parallel to buoyancy contours as has already been noted. This phenomenon also occurs when explicit diffusion is present. When explicit diffusion is included and after the initial drop, there are two distinct phases in the decay of the total variance. After about 15 days, there is an increase in the decay rate; after this time, the total variance in the two models decay at nearly the same rate. The decay rate in the earlier stage is greater in the results of the unmodified model. An examination of the temperature data shows that the most severe overshoot in the unmodified code occurs in the first 10–15 days. After 15 days, explicit diffusion has smoothed out the overshoot. The enhanced decay in the early stages of the flow development reflects the enhanced explicit diffusion due to the artificially large gradients generated by overshoot and demonstrates the mechanism already mentioned. Note that the curves in Fig. 10 are for the total variance, but the enhanced explicit diffusion is a local phenomenon and thus will be much more pronounced in regions of high overshoot. After about ten days, the effects of numerical diffusion are much less than those of explicit diffusion and also less than the enhanced explicit diffusion that occurs in the first 10 days. In the case of the ocean model above, the standard advection scheme continues to generate under- and overshoot throughout the entire calculation; therefore, the enhanced explicit diffusion is always present.

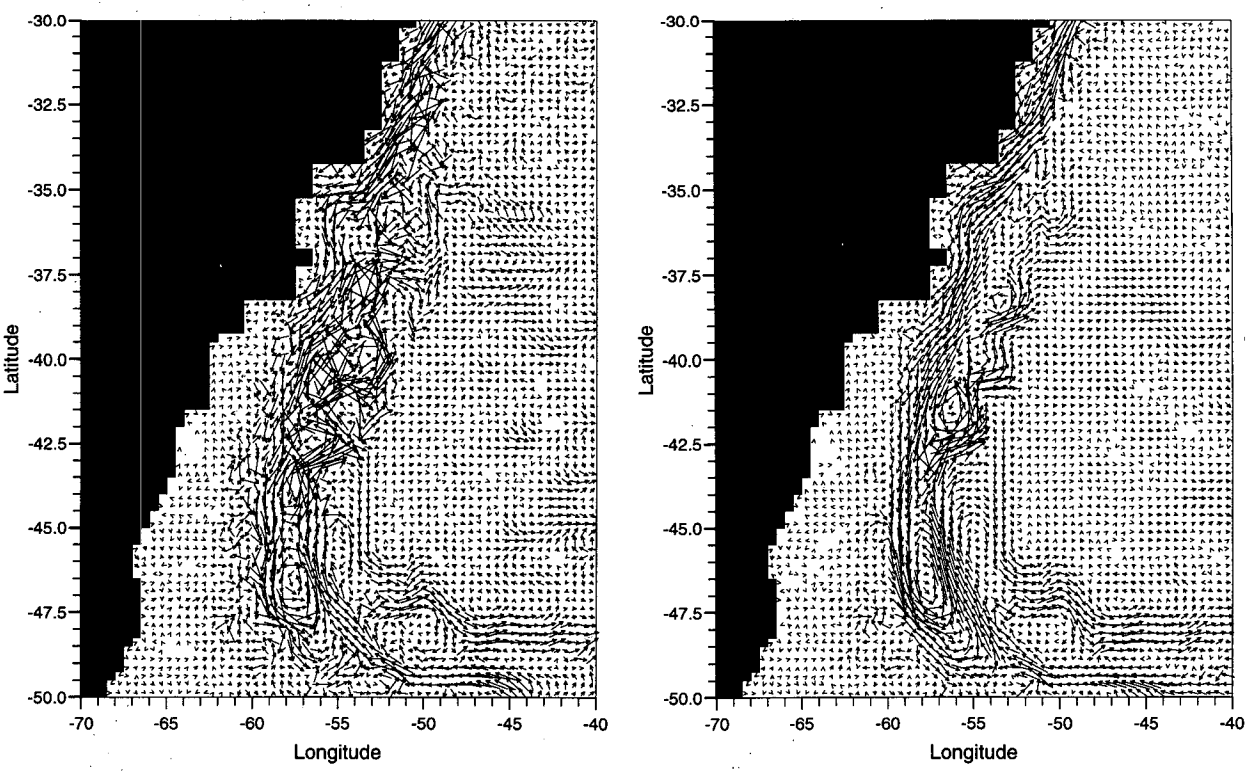

FIG. 8. Surface current vectors after 100 days as calculated by (a) the standard code and (b) the modified code.

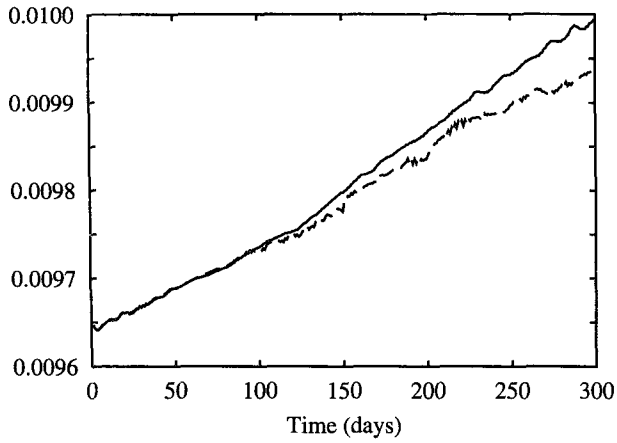

FIG. 9. Time series of the total variance of the temperature as calculated by the two codes. The solid line is for the modified model and the dashed is for the standard model.

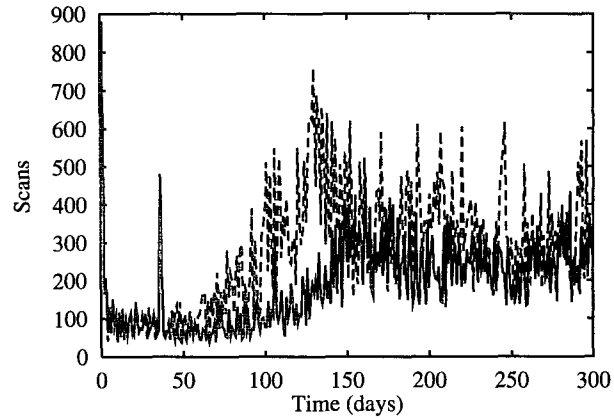

FIG. 11. Time series of the total number of scans used in calculating the barotropic streamfunction. The solid curve is the modified model and the dashed line is the standard model.

4. Concluding remarks

The QUICK advection scheme of Leonard (1979) has been adapted for use within the tracer component of a Bryan–Semtner–Cox type ocean general circulation model. The scheme significantly reduces the under- and overshoot associated with the more usual centered spatial differencing of the advection terms. Note, however, that the under- and overshoot has not been eliminated entirely, and the advection scheme described in this paper would not be appropriate where a positive definite scheme is required.

The reduction in the under- and overshoot has been achieved with only a moderate increase in computational cost. Simulations using the new model can take as little as 10% longer than the unmodified model. This is despite the new advection scheme involving two sweeps through the tracer fields at each time step. The reason for this small increase can be seen in Fig. 11, where a time series of the total number of scans used in calculating the barotropic streamfunction is shown. For the unmodified model, the over- and undershoot generates a noisy buoyancy field, which means that it takes longer to solve for the streamfunction. Other models use more direct methods to calculate the barotropic mode—for example, the free surface formulation of Killworth et al. (1991). We estimate that the increase in computation time associated with using the new advection scheme in such a model is approximately 25%.

The new scheme introduces some numerical diffusion, but this extra diffusion is less than the enhanced explicit diffusion that is associated with centered spatial differencing. The new scheme will be used in the high-resolution global model of the OCCAM (Ocean Circulation and Climate Advanced Modelling) group.

Acknowledgments. The authors thank D. Webb, P. Killworth, S. Maskell, and the anonymous reviewers for their valuable comments on earlier versions of this manuscript, and J. Johnson for useful discussions regarding this work. The research was supported by UK NERC Grant GR3/8526.

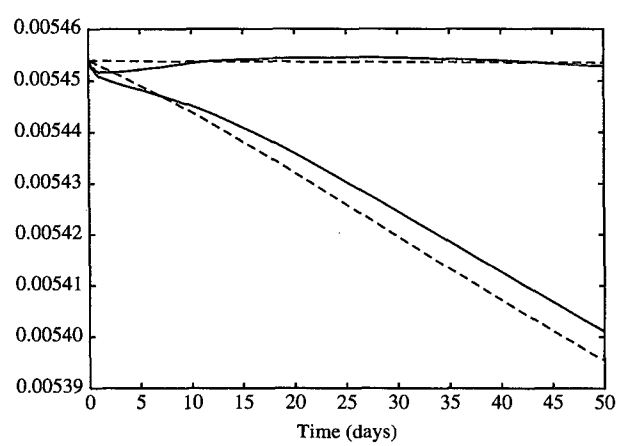

FIG. 10. Times series of the total variance of the temperature in the idealized model with and without explicit diffusion. The solid line is for the modified model and the dashed is for the standard model. The upper two curves are with no explicit diffusion.

APPENDIX

Generalization of Scheme for Ocean Model

To include the new scheme in an ocean model, the finite-difference equations (3) need to be generalized to account for a nonuniform grid (in particular, in the vertical coordinate) and a velocity field that varies with space and time. The advective flux into each control volume is decomposed into three components, one for each coordinate direction. Only one component is treated here (called x) with the tracer value S_i^n being stored at the grid point x_i, which is taken to lie in the geometric center of its control volume. The velocity at

the left wall of the control volume at time level n is denoted by u_l^n, while that at the right wall is denoted by u_r^n. These velocities are treated as "given."

For the predictor stage, the tracer values at the $n + 1/2$ time level are calculated using

$$S_i^{n+1/2} = S_i^n - \frac{\Delta t}{2}\left(u_r^n \frac{\Delta x_{i+1} S_i^n + \Delta x_i S_{i+1}^n}{\Delta x_{i+1} + \Delta x_i} - u_l^n \frac{\Delta x_i S_{i-1}^n + \Delta x_{i-1} S_i^n}{\Delta x_{i-1} + \Delta x_i}\right), \quad \text{(A1)}$$

where $\Delta x_i = x_i - x_{i-1}$ and Δt is the time step. For a uniform spatial discretization, the above equation reduces to

$$S_i^{n+1/2} = S_i^n - \frac{\Delta t}{2}\left(u_r^n \frac{S_i^n + S_{i+1}^n}{2} - u_l^n \frac{S_{i-1}^n + S_i^n}{2}\right). \quad \text{(A2)}$$

The form for the corrector step depends on the sign of the velocities u_l^n and u_r^n. In any case, S_i^n can be written

$$S_i^{n+1} = S_i^n - \Delta t\left(u_r^{n+1/2}\left[\frac{\Delta x_{i+1} S_i^{n+1/2} + \Delta x_i S_{i+1}^{n+1/2}}{\Delta x_{i+1} + \Delta x_i} - \frac{1}{8}\mathrm{CURV}_r^{n+1/2}\right] - u_l^{n+1/2}\left[\frac{\Delta x_i S_{i-1}^{n+1/2} + \Delta x_{i-1} S_i^{n+1/2}}{\Delta x_{i-1} + \Delta x_i} - \frac{1}{8}\mathrm{CURV}_l^{n+1/2}\right]\right), \quad \text{(A3)}$$

where

$$\mathrm{CURV}_l^{n+1/2} = \begin{cases} \dfrac{8\Delta x_{i-1}\Delta x_i}{\Delta x_{i-2} + 2\Delta x_{i-1} + \Delta x_i}\left(\dfrac{S_i^{n+1/2} - S_{i-1}^{n+1/2}}{\Delta x_{i-1} + \Delta x_i} - \dfrac{S_{i-1}^{n+1/2} - S_{i-2}^{n+1/2}}{\Delta x_{i-2} + \Delta x_{i-1}}\right) & u_l > 0, \\ \dfrac{8\Delta x_{i-1}\Delta x_i}{\Delta x_{i-1} + 2\Delta x_i + \Delta x_{i+1}}\left(\dfrac{S_{i+1}^{n+1/2} - S_i^{n+1/2}}{\Delta x_i + \Delta x_{i+1}} - \dfrac{S_i^{n+1/2} - S_{i-1}^{n+1/2}}{\Delta x_{i-1} + \Delta x_i}\right) & u_l < 0 \end{cases} \quad \text{(A4)}$$

and

$$\mathrm{CURV}_r^{n+1/2} = \begin{cases} \dfrac{8\Delta x_i\Delta x_{i+1}}{\Delta x_{i-1} + 2\Delta x_i + \Delta x_{i+1}}\left(\dfrac{S_{i+1}^{n+1/2} - S_i^{n+1/2}}{\Delta x_i + \Delta x_{i+1}} - \dfrac{S_i^{n+1/2} - S_{i-1}^{n+1/2}}{\Delta x_{i-1} + \Delta x_i}\right) & u_r > 0, \\ \dfrac{8\Delta x_i\Delta x_{i+1}}{\Delta x_i + 2\Delta x_{i+1} + \Delta x_{i+2}}\left(\dfrac{S_{i+2}^{n+1/2} - S_{i+1}^{n+1/2}}{\Delta x_{i+1} + \Delta x_{i+2}} - \dfrac{S_{i+1}^{n+1/2} - S_i^{n+1/2}}{\Delta x_i + \Delta x_{i+1}}\right) & u_r < 0 \end{cases} \quad \text{(A5)}$$

and

$$u_{[l,r]}^{n+1/2} = (u_{[l,r]}^n + u_{[l,r]}^{n+1})/2. \quad \text{(A6)}$$

For a uniform spatial discretization, the above equations reduce to

$$\mathrm{CURV}_l^{n+1/2} = \begin{cases} S_i^{n+1/2} - 2S_{i-1}^{n+1/2} + S_{i-2}^{n+1/2} & u_l > 0, \\ S_{i+1}^{n+1/2} - 2S_i^{n+1/2} + S_{i-1}^{n+1/2} & u_l < 0 \end{cases} \quad \text{(A7)}$$

and

$$\mathrm{CURV}_r^{n+1/2} = \begin{cases} S_{i+1}^{n+1/2} - 2S_i^{n+1/2} + S_{i-1}^{n+1/2} & u_r > 0, \\ S_{i+2}^{n+1/2} - 2S_{i+1}^{n+1/2} + S_i^{n+1/2} & u_r < 0. \end{cases} \quad \text{(A8)}$$

For the purposes of the ocean model, if the calculation of the CURV terms involves a grid point outside the domain, the CURV correction is ignored; that is, a linear interpolation is used.

REFERENCES

Arakawa, A., 1966: Computational design for long-term numerical integration of the equations of fluid motion: Two-dimensional incompressible flow. Part 1: *J. Comput. Phys.*, **1**, 119–143.

Boris, J. P., and D. L. Book, 1973: Flux-corrected transport. Part 1: SHASTA, a fluid transport algorithm that works. *J. Comput. Phys.*, **11**, 38–69.

Bryan, F. O., and W. R. Holland, 1989: A high resolution simulation of the wind- and thermohaline-driven circulation in the North Atlantic Ocean. *Parameterization of Small-Scale Processes. Proceedings of the 'Aha Huliko'a Hawaiian Winter Workshop,* P. Muller and D. Henderson, Eds., University of Hololulu, 99–115.

Bryan, K., 1969: A numerical model for the study of the circulation of the World Ocean. *J. Comput. Phys.*, **4**, 347–376.

Cox, M. D., 1984: A primitive equation three-dimensional model of the ocean. GFDL Ocean Group Tech. Rep. No. 1, GFDL/NOAA, Princeton University, Princeton, NJ, 250 pp.

FRAM Group, 1991: An eddy-resolving model of the Southern Ocean. *Eos, Trans. Amer. Geophys. Union,* **72**(15), 169, 174–175.

Gerdes, R., C. Köberle, and J. Willebrand, 1991: The influence of numerical advection schemes on the results of ocean general circulation models. *Climate Dyn.*, **5**, 211–226.

Killworth, P. D., D. Staniforth, D. J. Webb, and S. Paterson, 1991: The development of a free surface Bryan–Cox–Semtner model. *J. Phys. Oceanogr.*, **21**, 1333–1348.

Leonard, B. P., 1979: A stable and accurate convective modelling procedure based on quadratic upstream interpolation. *Comput. Methods Appl. Mech. Eng.*, **19**, 59–98.

——, and H. S. Niknafs, 1991: Sharp monotonic resolution of discontinuities without clipping of narrow extrema. *Comput. Fluids,* **19**, 141–154.

Levitus, S., 1982: Climatological atlas of the world ocean. NOAA Professional Paper, 13, U.S. Dept. of Commerce, 173 pp.

Matano, R. P., 1993: On the separation of the Brazil Current from the coast. *J. Phys. Oceanogr.*, **23,** 79–90.

Pacanowski, R. C., K. Dixon, and A. Rosati, 1991: The GFDL Modular Ocean Model users guide. GFDL Ocean Group Tech. Rep. No. 2, 24 pp.

Patankar, S. V., 1988: Recent developments in computational heat transfer. *Trans. ASME, J. Heat Transfer,* **110,** 1037–1045.

Rood, R. B., 1987: Numerical advection algorithms and their role in atmospheric transport and chemistry models. *Rev. Geophys.*, **25,** 71–100.

Semtner, A. J., 1974: An oceanic general circulation model with bottom topography. UCLA Department of Meteorology Tech. Rep. No. 9, 99 pp.

——, and R. M. Chervin, 1992: Ocean general circulation from a global eddy-resolving model. *J. Geophys. Res.*, **97,** 5493–5550.

Staniforth, A., and J. Côté, 1991: Semi-Lagrangian integration schemes for atmospheric models—a review. *Mon. Wea. Rev.*, **119,** 2206–2223.

Webb, D. J., 1993: An ocean model code for array processor computers. Institute of Oceanographic Sciences, Deacon Laboratory, Internal document, No. 324, 21 pp.

——, P. D. Killworth, A. C. Coward, and S. R. Thompson, 1991: The FRAM atlas of the Southern Ocean. Natural Environment Research Council, Swindon, U.K., 67 pp.